MANIPULATION OF RARE CELLS IN MICROFLUIDIC DEVICES USING MAGNETOPHORESIS AND DIELECTROPHORESIS BASED ON COMPOSITE-PDMS

Julien Marchalot, Renaud Gelszinnis, A.-L. Deman, Magalie Faivre, Jean-François Chateaux, Charlotte Rivière, Hichem C Mertani, Rosaria Ferrigno

DRAFT μFLU14-2014/78

MANIPULATION OF RARE CELLS IN MICROFLUIDIC DEVICES USING MAGNETOPHORESIS AND DIELECTROPHORESIS BASED ON COMPOSITE-PDMS

Julien Marchalot[1], Renaud Gelszinnis[1], Anne-Laure Deman[1] , Magalie Faivre[1], Jean-François Chateaux[1], Charlotte Rivière[2], Hichem Mertani[3] Rosaria Ferrigno[1*]

[1]Institut des Nanotechnologies de Lyon, INL, CNRS UMR 5270, Université de Lyon, Lyon, F-69003, France
julien.marchalot@univ-lyon1.fr, renaud.gelszinnis@univ-lyon1.fr, anne-laure.deman-him@univ-lyon1.fr, magalie.faivre@univ-lyon1.fr, jean-francois.chateaux@univ-lyon1.fr
2 Institut Lumière Matière, ILM, CNRS UMR 5306, Université de Lyon,
Lyon, F-69003, France
charlotte.riviere@univ-lyon1.fr
3 Centre de Recherche en Cancérologie de Lyon, UMR INSERM U1052 CNRS UMR5286, France
hichem.mertani@lyon.unicancer.fr

KEY WORDS

Lab-on-a-Chip, capture, separation, composite-PDMS, dielectrophoresis, magnetophoresis.

ABSTRACT

Enrichment of rare cell populations, such as Circulating Tumor Cells (CTCs) or parasitized Red Blood Cells (RBCs), is a tremendous challenge. Indeed, technologies must be able to reach high both purity and recovery rates while keeping the cells intact for downstream analysis. Two main approaches, affinity-based and label-free methods, have already been demonstrated in microfluidic format. Among them, the use of field gradients, electrical field for dielectrophoresis and magnetic field for immuno-magnetic separation, has gained a large interest. This paper demonstrates that PDMS-based composite materials present many advantages over metallic microstructures for the fabrication of active microfluidic devices. Indeed, we showed that these materials, combining properties of both the matrix and doping particles, allows the easy and fast integration of metallic microstructures using soft-lithography approach while preserving O_2 plasma bonding properties of PDMS substrate and avoiding cumbersome alignment procedure. Here, we focused on two different composites: (i) PDMS doped with carbon nanoparticles (C-PDMS) to obtain conductive polymer and (ii) PDMS doped with iron carbonyl microparticles (i-PDMS) to give this composite, ferromagnetic properties. We demonstrated that 3D conductive or ferromagnetic microstructures were easily obtained. C-PDMS electrodes showed dielectrophoresis capture of CTCs from a flowing model blood sample hence highlighting the interest of the composite material. Similarly, i-PDMS allowed the trapping of magnetically labelled cancer cells flowing at its vicinity, thanks to the generation of high magnetic field gradient.

1. INTRODUCTION

Cells at very low concentration, typically less than 1000 target cells per milliliter of body fluids, are considered as circulating rare cells or low-abundance cells. A typical example is Circulating Tumor Cells (CTCs) that are at a concentration as low as 1 to 100 CTCs/mL of peripheral blood from a human cancer patient. Enumeration of such rare cells presents medically important applications such as in cancer diagnosis and prognosis, non-invasive prenatal diagnosis and cell-based therapies. Therefore, there is a tremendous challenge[1] in the development of technologies and devices able to manipulate them, more specifically to enrich, capture, separate them from a sample containing a large amount of other cells. Such technologies must demonstrate high purity and recovery rate while keeping the cells intact for downstream analyses. Two main approaches, affinity-based[2-4] and label-free[5-7] methods, have already been demonstrated in microfluidic format. For both approaches, the use of field gradient, electrical field for dielectrophoresis

* Corresponding author

(DEP) and magnetic field for immuno-magnetic separations, has gained a large interest[8]. However, to be applied to real clinical samples and become commercial products, these devices and methodologies still need development. The generation of controlled field gradient in microfluidic format necessitates the integration of heterogeneous materials. Indeed, although most of the microfluidic systems are fabricated in polymer materials, microsystems integrating active functions - requiring the generation of either magnetic or electric field gradients - necessitates the integration of metallic materials in these polymers. Poly-DimethylSiloxane (PDMS) is largely exploited in microfluidic devices due to its biocompatibility, optical properties and ease of microstructuration. However, the combination of PDMS with other materials can be challenging, as ferromagnetic and conductive materials cannot be efficiently sealed to PDMS using simple O_2 plasma treatment. This heterogeneous integration can result in tightness issue and be very cumbersome when precise alignment is required. Moreover, it has been shown that the integration of 3D microstructures can improve active function performances[9-11]. However, 3D microstructure fabrication and integration are more challenging than conventional 2D coplanar patterns.

The objective of this proceeding is to demonstrate that the implementation of composite PDMS materials can be a simple and efficient method to circumvent previous challenges. These materials, which are composed of a PDMS matrix doped with nano- and/or microparticles, present new properties compared to the native PDMS. In our case, we focused on two different composites: (i) PDMS doped with carbon nanoparticles (C-PDMS) to obtain conductive polymer[12] and (ii) PDMS doped with iron carbonyl microparticles (i-PDMS) to give this composite, ferromagnetic properties[13]. First, we report on the technological process developed to integrate composite-PDMS microstructures into microfluidic channels and then, demonstrate their DEP and magnetophoretic functionalities.

2. EXPERIMENTAL SECTION

2.1 Preparation of Composite-PDMS Material

Two different dopant particles were used in this work: (i) carbon black nanoparticles (20 to 60 nm in diameter, Vulcan XC72-R, Cabot Inc.) to prepare C-PDMS and (ii) carbonyl iron microparticles (dry powder, 7 μm diameter, 97% Fe basis, Sigma-Aldrich) for i-PDMS. Particles and PDMS mixture (10/1 w/w of monomer and curing agent respectively, Silgard from Samaro) were thoroughly mixed (4-15 min) in a mortar until obtaining an homogeneous paste before reticulation. Based on previous results[12, 13], we used optimum particle concentration in order to achieve the highest material characteristics while preserving its capacity to be molded. These concentrations were 25% w/w for C-PDMS to reach a conductivity of 10 S m^{-1} and 83% w/w for i-PDMS attaining a magnetic relative permittivity μ_r of 2.28. These values were comparable to the values obtained in other references[14,15] but are still lower than bulk materials. Although they were sufficient to give to composite-PDMS new functionalities, it will be interesting in the future to investigate other dopants (particle size, shape and nature) in order to improve their characteristics.

2.2 Fabrication of the Microfluidic Devices

Microfluidic devices were prepared by using a soft-lithography approach. In our case (Fig. 1), the process was composed of three successive steps. First, the mold was obtained using photolithography (Fig. 1 (a) and (b)). Then, composite-PDMS paste was plastered on dedicated areas of the master (Fig. 1 (c)). After cleaning eventual excess of composite-PDMS, the composite was baked in an oven (75°C, 60 min). Then, pure PDMS was poured on the top of the whole master and the whole system was baked (75°C, 60 min) a second time in order to cure pure PDMS. Composite-PDMS/PDMS slab was then peeled off from the master and bound by O_2 plasma to a glass slide.

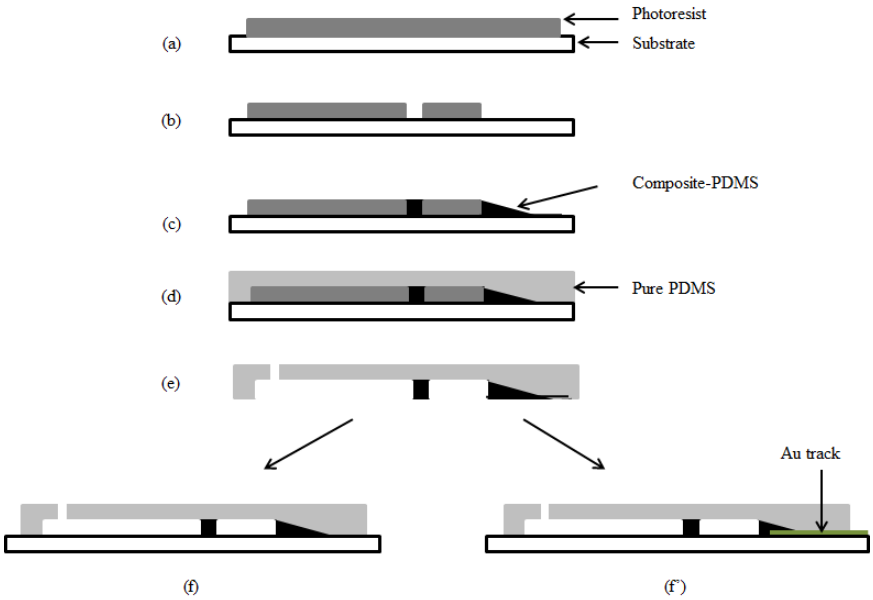

Figure 1: Schematic representation of the fabrication process developed to integrate composite-PDMS microstructures in a PDMS microfluidic channel. (a) the substrate was coated with a photoresist layer, (b) the master was obtained for replication, (c) the composite-PDMS was plastered and cured, (d) pure PDMS was poured and cured, (e) the PDMS slab was peeled off and inlets and outlets were punched, (f) and (f') the PDMS slab was then bound to a glass slide by O_2 plasma (in the case of C-PDMS, the glass slide was pre-patterned with Au tracks to achieve electrical connections between C-PDMS electrodes and Cu wires soldered to Au tracks).

As presented in Fig. 2, two different microfluidic configurations were designed in order to demonstrate DEP and magnetophoresis functions using composite material. In the case of DEP configuration (Fig. 2a), two C-PDMS electrodes (50 or 100 μm thick) were embedded in channels having walls of identical thickness (50 or 100 μm). We used two electrode geometries: (i) a geometry where electrodes were face-to-face and (ii) one where electrodes were shifted. In both cases, the channel width was 500 μm and the minimal distance between the electrodes was 200 μm. The shape of the electrodes were right-angle isoscele triangles with a height of 150 μm. At a concentration of 25 wt%, C-PDMS is a viscous, paste-like material, that is not easily patterned in acute angles. In this work, we chose the shape of the triangular electrodes in order to limit problems of reproducibility during fabrication. In the case of i-PDMS, the viscosity being lower, we managed to design i-PDMS microstructures down to 50 μm[13]. However, in magnetophoresis configuration (Fig. 2 (b)), we designed a 45 μm thick and 1000 μm wide PDMS microchannel incorporating in the center of the channel 20 diamond shape i-PDMS microstructures (500 μm wide and 45 μm thick).

2.3 Cell Preparation

MDA-MB-231, MCF7, HBL100 are immortalized cell lines of human breast cancer. Cells were grown in Dubelcco's Modified Eagle Medium (DMEM) supplemented with 10% fetal bovine serum (FBS) and 1% penicillin-strptomycin (PS). Cells were incubated in a 5% CO_2 and 95% O_2 atmosphere at 37°C. When necessary, cells were collected after upon trypsin incubation, washed and suspended in the appropriate medium.

For DEP experiments, after collect, cells were centrifuged twice in DMEM and then suspended in DEP buffer composed of 8.5% (w/v) sucrose, 0.3% (w/v) glucose and 0.7% (v/v) DMEM in distilled water. Conductivity and pH of this buffer were respectively 100 μS/cm and 7. Cells concentration were typically in the range of 4-8$\times 10^6$ /mL. CTCs experiments were performed using a mixture of MDA-MB-231 and Red Blood Cells (RBCs) as a model. Peripheral blood samples were collected from healthy donor from Etablissement Français du Sang (EFS). RBCs were separated from white blood cells and platelets by centrifugation in Phosphate Saline Buffer solution (PBS) and then diluted with DEP buffer at a concentration of 50$\times 10^6$ /mL. MDA-MB-231 and RBCs were finally mixed at a ratio of 1:10.

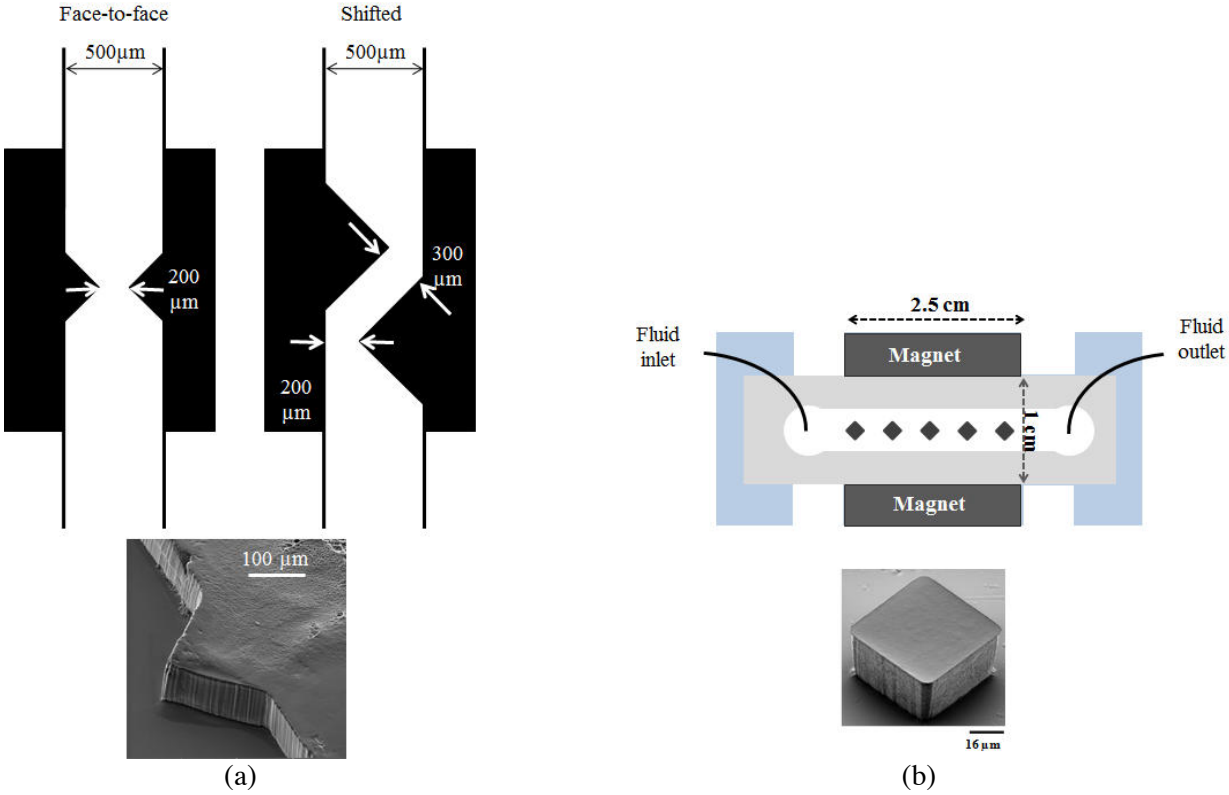

Figure 2: (a) DEP configuration in face-to-face and shifted designs featuring embedded C-PDMS electrodes, a SEM image is provided to show detail of the tip of the C-PDMS electrodes), (b) magnetophoresis configuration with i-PDMS diamond microstructures, a SEM image is provided to show detail of a i-PDMS microstructure.

For magnetophoresis experiments with magnetically labelled cells, we used GFP modified MDA-MB-231. These cells were labeled with a suspension of maghemite nanoparticles provided by C. Ménager (Laboratoire PESCA, UMR7195, Université Paris 6, France) and were treated as described elsewhere[13]. Samples injected in the microsystem were at the concentration of 6×10^6 /mL. In preliminary experiments, we used microbeads to model cell behaviours. Magnetically labelled cells were modeled by 12 μm in diameter superparamagnetic microparticles (magnetite in a polystyrene copolymerisate) whereas unlabeled cells were modeled using 10 μm in diameter non-magnetic fluorescent microparticles. These particles were suspended at a concentration of 160 /μL in filtered PBS with 3.6% w/w dextran (Mw = 2×10^6 leuconostoc spp. From Sigma Life Science). Dextran was used to reduce sedimentation of the particles during the time of the experiment.

2.4 Experimental Set-Up

Microsystems were placed on an inverted epifluorescence microscope (LEICA DMI4000B) and a camera (LEICA DFC340 FX) was used for data acquisition. Image J® was used to perform image analysis and to retrieve bead and cell trajectories. Before operation, microsystems were passivated with 2% bovine Serum Albumin (BSA) in PBS in order to avoid any non-specific adsorption and then rinsed with PBS. A syringe pump (Harvard Apparatus) was used to inject the solutions.
Electrical fields were supplied through a waveform generator (Agilent 33521A) and a High Voltage Amplifier (FLC Electronics Voltage Amplifier A800) connected to the microsystems. In this work, the voltage used for DEP experiments are expressed as pea-to-peak voltage.
For magnetophoresis experiments, the external magnetic field was generated by two permanent magnets (Nd/Fe/Br $25\times10\times5$ mm^3, 1.2 T at the pole, polarization in the longest dimension) whose position was secured in a home-made plastic holder. Relative position of the magnets and microfluidic channel was optimized elsewhere[13] at a value of 10 mm .

3. RESULTS AND DISCUSSION

3.1 DEP Capture Using C-PDMS Electrodes

When subjected to a gradient of electrical field, a dielectric particle, such as a biological cell, experiences a DEP force expressed as:

$$\mathbf{F}_{\mathrm{DEP}} = 2\pi\varepsilon_m r^3 \,\mathrm{Re}\left(f_{CM}\right)\nabla\mathbf{E}^2 \qquad (1)$$

where ε_m is the permittivity of the medium, r is the particle radius, $\mathrm{Re}\left(f_{CM}\right)$ the real part of the Clausius-Mosotti (CM) factor and $\nabla\mathbf{E}^2$ is the gradient of the square norm of the electric field. The CM depends on the frequency and is defined by:

$$f_{CM} = \frac{\varepsilon_p^* - \varepsilon_m^*}{\varepsilon_p^* + 2\varepsilon_m^*} \qquad (2)$$

where subscript term p, respectively m, refers to the particle, respectively to the medium and the term ε^* is the complex permittivity described as $\varepsilon^* = \varepsilon - \frac{j\sigma}{\omega}$ with ε the permittivity, σ the conductivity, ω the angular frequency and $j = \sqrt{-1}$.

When flowing in microfluidic channel, particles are also subjected to the drag force defined by Stokes' law:

$$\mathbf{F}_{drag} = 6\pi\eta r\left(\mathbf{v}_f - \mathbf{v}_p\right) \qquad (3)$$

where η is the fluid viscosity, v_p the velocity of the particle and v_f the fluid velocity.

We demonstrated in previous works the capacity of C-PDMS electrodes embedded in PDMS microchannel to carry out DEP and electrical lysis[12,16] in stagnant mode. However, these results were obtained using parallel plane electrodes where gradient of electrical field where induced by electrode roughness and therefore were not adapted for rare cell capture. Here, we used geometries as presented in Fig. 2(a) in order to quantify cell capture yield (defined as the ratio between the number of captured target cell to the total number of target cells flowing) of MDA-MB-231 cancerous cells. On the application of the electric field (3.75 kV/cm 1 MHz), MDA-MB-231 cells flowing in both geometries were captured at the tips of the C-PDMS electrodes as shown in Fig. 3 (a). First, we evaluated the yield for 50 μm thick electrodes embedded in two microchannel geometries, face-to-face and shifted. As presented in Fig. 3 (b), for both geometries, the yield decreases with flow rate. For, face-to-face, it decreases from 80 to 40 % as the flow rate is increased from 10 to 40 μL/h. Indeed, the increase of the flow rate results in the increase of the drag force for a constant DEP force. We can also notice that in the case of the shifted geometry, the yield remains larger than in the face-to-face one. In this case, the yield is 94% at 10 μL/h and 67% at 40 μL/h. Therefore, the shifted geometry exhibits a larger influence zone (zone where $\mathbf{F}_{\mathrm{DEP}} > \mathbf{F}_{drag}$) than the face-to-face geometry. Even if capture yield is an important figure of merit for rare cell capture, the throughput must also be sufficiently high in order to treat a large volume of sample in a minimum of time. We show in Fig. 3 (c) that by using thicker electrodes (100 μm), it is possible to maintain a large yield for higher flow rate. Indeed, this yield ranges from 96% to 79% for flow rates ranging from 10 to 80 μL/h. We can deduce that thanks to 3D C-PDMS electrodes, DEP capture throughput can be increased while keeping a large capture yield. This yield is in the same order of magnitude as previously published works[17] where yield ranges from 60 to 96% at flow rates ranging from 1 mL/h to 6 μL/h.

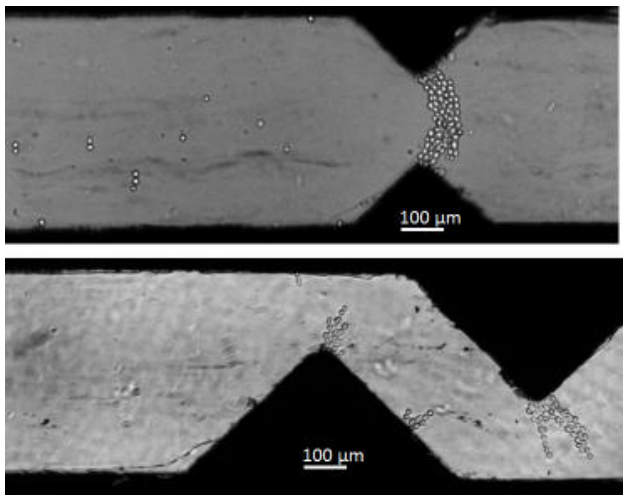

(a)

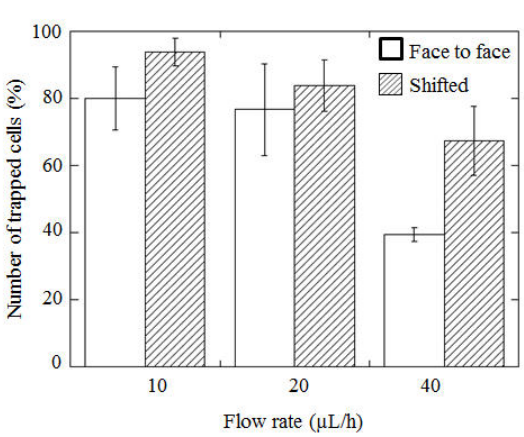

(b)

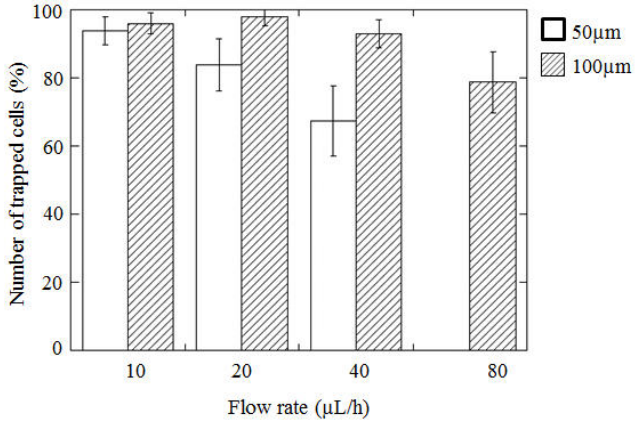

(c)

Figure 3: (a) Optical image of captured MDA-MB-231 cancerous cells at the tip of C-PDMS electrodes in face-to-face (flow rate of 15 μL/h) and shifted geometries (flow rate of 40 μL/h with 50 μm thick channel), (b) Evolution of capture yield of MDA-MB-231 cells as a function of flow rate for the 50 μm thick face-to-face and shifted configurations, (c) Evolution of capture yield of MDA-MB-231 cells as a function of flow rate for 50 and 100 μm thick shifted configuration. DEP parameters were an applied electric field of 3.75 kV/cm at 1 MHz.

The increase of throughput can also be obtained using parallelization. In Fig. 4 (a), we used a bipolar configuration to trap cells in parallel microchannels using a minimum of electrical connections. This preliminary experiment demonstrated that we were able to capture HBL-100 and MCF7 cancerous cells in parallel with MDA-MB-231. In this experiment, as the DEP electrodes were associated in series (bipolar configuration), we used in order to capture cells the maximum voltage available with our instrumentation, *i.e.* 800 Vpp corresponding to an electric field of 6.7 kV/cm per channel. This value is larger than the value used to perform capture in a single channel. We assume that this bipolar configuration, where three microchannels are in parallel, increases ohmic losses and therefore only part of the electric field was used to perform DEP. In future, it will be interesting to investigate capture yield and throughput of such a microdevice while trying to reduce ohmic losses. We also carried out qPCR on cells lysated on-chip after DEP capture in order to demonstrate that molecular integrity was conserved. We were able to detect MCF7 and MDA-MB-231 specific markers (ER1 receptor and vimentin) in the lysate sample. DEP capture using our approach is therefore adapted for molecular downstream analyses. Finally, preliminary results on the capture of MDA-MB-231 mixed with RBCs suspension for a CTCs concentration ratio of 1:10 are shown in Fig. 4 (b). In this figure, we can clearly observe the capture of cancerous cells at the tip of the C-PDMS electrode while RBCs are flowing along the fluid stream. To be captured, cancerous cells were attracted by the gradient of electrical field (0.75 kV/cm at 140 kHz) arising at the electrode tip and were deviated from

their streamline path. Electrical field was chosen in order to minimize DEP force on RBCs ($\mathrm{Re}(f_{CM}) \approx 0.1$) and maximize this force on CTCs ($\mathrm{Re}(f_{CM}) \approx 0.5$). Future work will include the quantification of the capture yield in the case of a mixture of cancerous cells (MCF7, HBL-100 and MDA-MB-231 with RBCs).

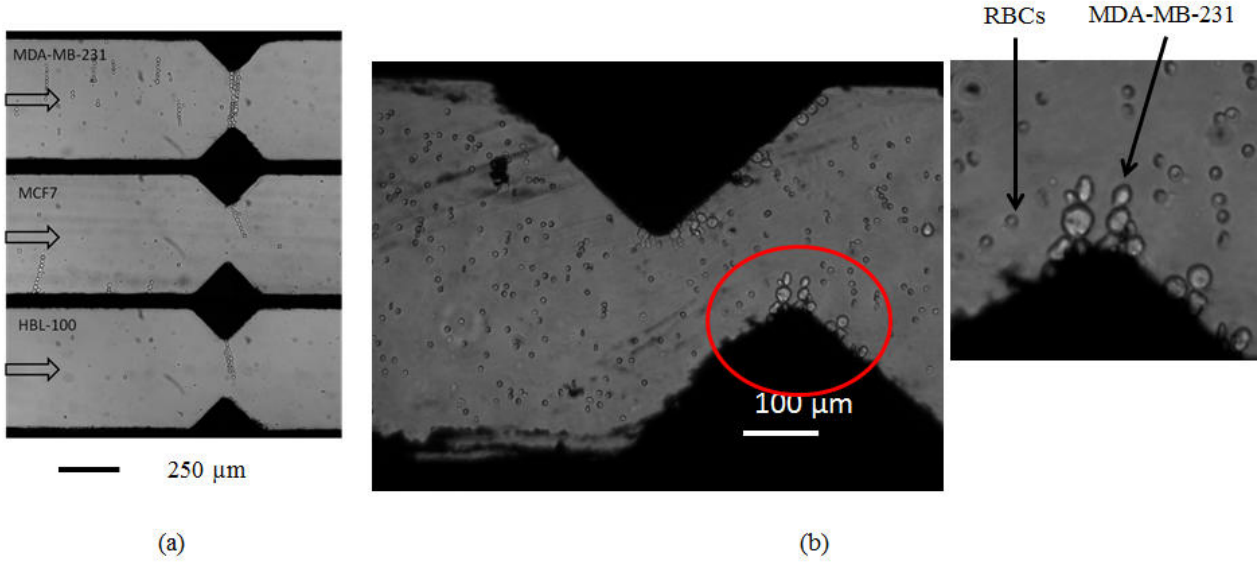

Figure 4: (a) Optical image showing three pairs of C-PDMS electrodes connected in bipolar configuration in three parallel microchannels used for cancerous cell lines capture using DEP (6.7 kV/cm at 1 MHz, 20 μL/h), (b) optical image showing the capture of CTCs (MDA-MB-231) in RBCs flowing sample at 5 μL/h (parameters were 0.75 kV/cm at 140 kHz). Microchannels were 100 μm thick.

3.2 Magnetophoresis Capture Using i-PDMS Microstructures

When placed in a magnetic field gradient ($(\nabla.\mathbf{B})$, a magnetic microparticle is submitted to a magnetic force that is expressed as follow:

$$\mathbf{F}_{mag} = \frac{4\pi r^3}{3\mu_o}\Delta\chi(\mathbf{B}.\nabla)\mathbf{B} \qquad (4)$$

where r is the microparticle radius, $\mu_o = 4\pi.10^{-7}$ H.m^{-1} the vacuum permeability and $\Delta\chi = \chi_p - \chi_f$ represents the difference of magnetic susceptibilities between the particle (χ_p) and the surrounding fluid (χ_f).

Therefore, in a non-magnetic medium (such as water), the microparticle can be attracted or repelled by magnetic field gradient, depending on its magnetic properties. As for DEP, this force competes against hydrodynamic drag force as expressed in equation (3). The optimization of magnetophoresis capture by maximizing $\mathbf{F}_{mag}$ over $\mathbf{F}_{drag}$ have led to the integration in microfluidic channels of microstructures able to generate high spatially controlled gradient of magnetic field. We first demonstrated that i-PDMS, compared to pure PDMS, was able to generate such gradients using 12 μm superparamagnetic microparticles ($\chi_m = 8.44\times10^{-3}$) and non-magnetic particles. The beads were flowed at 50 μL/h in a PDMS microchannel containing 500 μm diamond i-PDMS structures. Fig. 5 presents a stack of videomicroscopy images that highlight particle trajectories. In absence of an applied magnetic field (Fig. 5 (a)), both paramagnetic and non-magnetic particles experienced only hydrodynamic force and therefore exhibited the same trajectories that illustrated the fluid velocity field lines. When placed in a magnetic field (Fig. 5 (b), trajectories were different. In the case of paramagnetic beads, we can observe that beads flowing sufficiently closed to i-PDMS microstructures were attracted towards them and were captured.

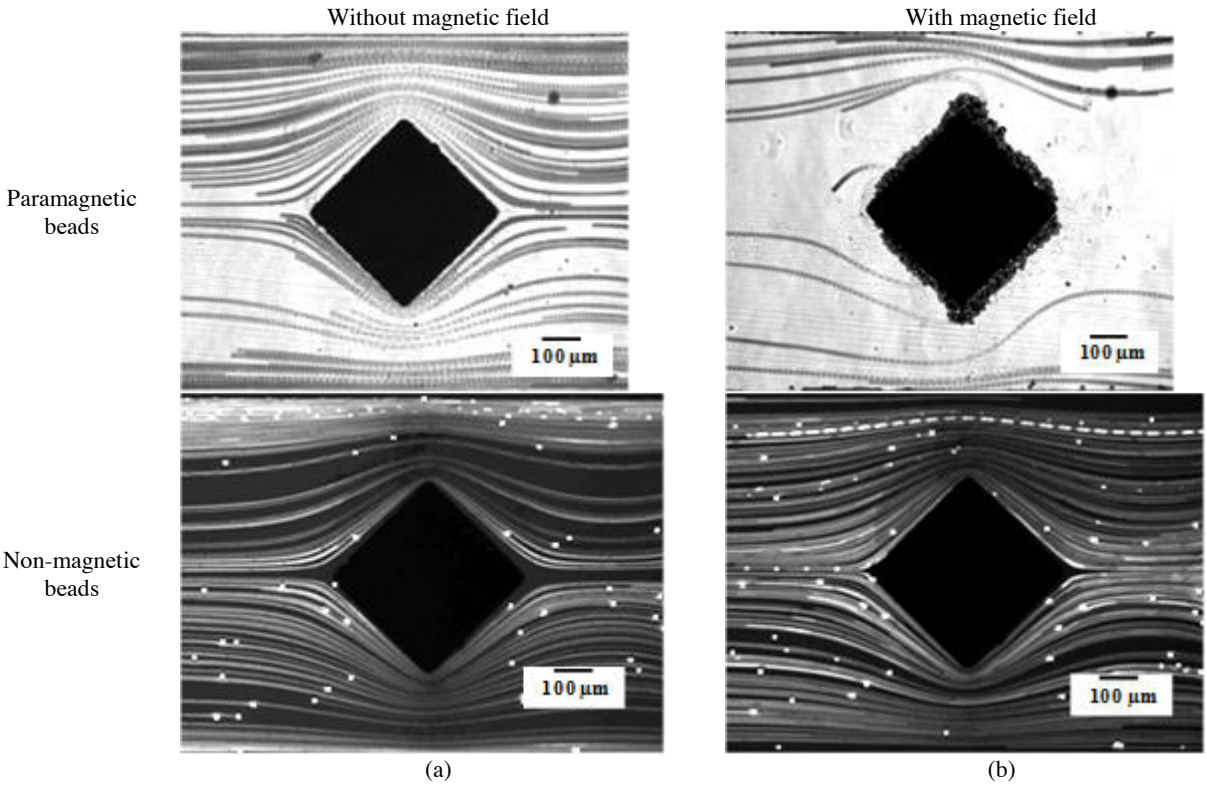

Figure 5: Z-stack projection of videomicroscopic images representing paramagnetic beads and non-magnetic beads flowing, under a flow rate of 50 μL/h, at the vicinity of an i-PDMS microstructure in absence (a) and in presence (b) of an external magnetic field.

Paramagnetic particles were experiencing a gradient of magnetic field generated by i-PDMS microstructure sufficiently large to outreach drag force. Particles flowing further away from the i-PDMS microstructures – i. e. closer to the channel walls - did not seem affected. Indeed, the gradient generated is local around the microstructures. In comparison, non-magnetic bead trajectories were not affected by the gradient. Then, we investigated the influence of flow rate on the capture yield. This yield was estimated by using the bead deviation defined by $\Delta Y = \left| Y_{upstream} - Y_{downstream} \right|$ where $Y_{upstream}$ is the y coordinate of the bead 500 μm upstream from the i-PDMS microstructure and $Y_{downstream}$ is the y coordinate of the bead 500 μm downstream from this microstructure (Fig. 6 (a)). Depending on this parameter, we defined three areas in the microchannel: (i) a capture area where all beads flowing were captured by the i-PDMS microstructure, (ii) a deviation area where beads were not captured but the magnetic force was sufficiently strong to deviate the beads resulting in $Y_{upstream} > Y_{downstream}$ and finally (iii) an area where beads were not affected by magnetic force.

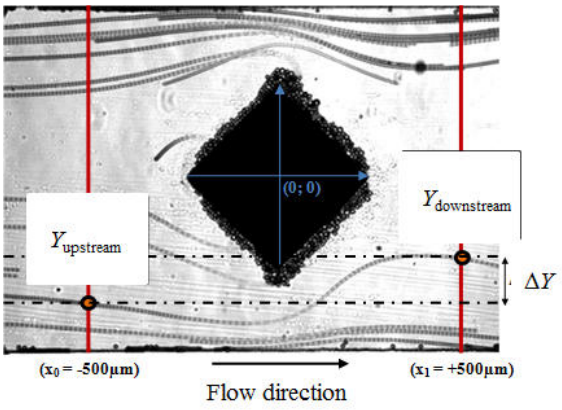

(a)

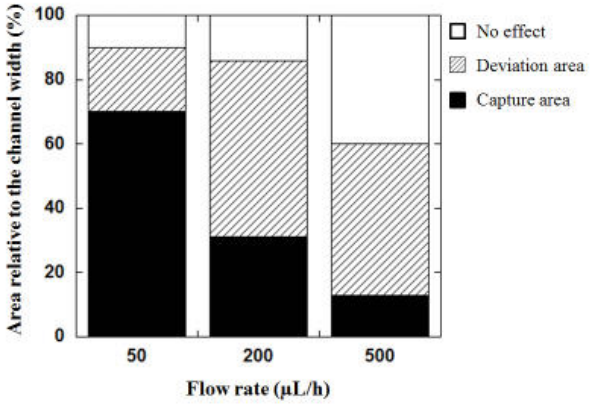

(b)

Figure 6: (a) Schematic representation explaining the measurement of the parameter $\Delta Y = \left| Y_{upstream} - Y_{downstream} \right|$. Y-positions of the beads were measured at two different locations : 500 µm respectively upstream ($Y_{upstream}$) and downstream ($Y_{downstream}$) from the center of the microstructure, allowing calculating the deviation of the bead, (b) Evolution of the measured deviation and capture areas as a function of the flow rate.

We investigated three different flow rates: 50, 200 and 500 μL/h in 45 μm high and 1 mm wide microchannel. The evolution of these area widths with the flow rate is presented in Fig. 6 (b). As expected, the increase of the flow rate results in the decrease of the capture area (from 70% to 13%) and the increase of the deviation area (from 20% to 47%). However, globally the influence of the i-PDMS microstructures was decreased as we can observe increase of the area where beads were not affected by the gradient of magnetic field. Finally, we tested the efficiency of our i-PDMS microstructures for the capture of magnetically labelled MDA cancerous cells (Fig. 7). As presented in Fig. 7, we can observe 5 i-PDMS microstructures located along the microfluidic channel. After injection, magnetically labelled cancerous cells were captured around the i-PDMS posts. Future works will have to evaluate the potential separation of cancerous cells flowing in blood. In this case, labelling of CTCs will be performed using antigen/antibody affinity between CTCs and magnetic nanoparticles.

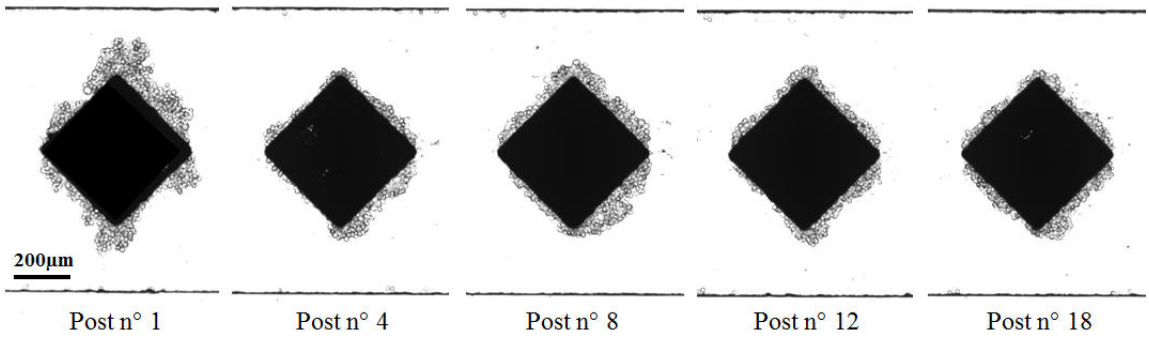

Figure 7: Bright field images of magnetically labeled cells captured on five different i-PDMS microstructure (post n°1, n°4, n°8, n°12 and n°18) in a microsystem integrating 20 i-PDMS microstructures

4. CONCLUSIONS

This paper demonstrates that PDMS-based composite materials present many advantages over metallic microstructures for the fabrication of active microfluidic devices. Indeed, we showed that these materials, combining properties of both the matrix and doping particles, allows the easy and fast integration of metallic microstructures using soft-lithography approach while preserving O_2 plasma bonding properties of PDMS substrate and avoiding cumbersome alignment procedure. We demonstrated that 3D conductive or ferromagnetic microstructures were easily obtained with respectively, C-PDMS and i-PDMS. Depending on

the doping agent properties (particle size, doping ratio), we managed to obtain structures of various shapes (triangles, squares and discs) with characteristic dimensions down to 50 µm using protocols based on replica molding adapted from soft-lithography. These microstructures were then integrated in microfluidic PDMS channels in order to evaluate their capacity for rare cell enrichment. C-PDMS was used to carry out dielectrophoresis isolation whereas i-PDMS was demonstrated suitable for magnetophoresis trapping. The principle of the DEP trapping system presented hereby was to create regions of high gradient of electric field and DEP traps at the tip of C-PDMS electrodes designed with triangular shape. We first highlighted the benefit of 3D electrodes embedded in microfluidic channel obtained easily thanks to C-PDMS composite to improve trapping efficiency. Metastatic breast cancer cells (MDA-MB-231) were injected in the different devices at flow rates ranging from 5 to 80 μL/h and the trapping yield was experimentally evaluated. Cell trapping yields of 97% at 20 μL/h and 78% at 80 μL/h were achieved for 100 μm thick C-PDMS electrodes. Preliminary results on the isolation of MDA-MB-231 from RBCs suspension for a CTCs concentration ratio of 1:10 were also obtained.
In the case of i-PDMS, we fabricated microsystems integrating 50 μm thick, diamond microstructures. We evaluated the magnetic trapping capacities of this material by injection of a suspension of superparamagnetic particles in the channel and obtained capture yield up to 70% at 50 μL/h with i-PDMS microstructures. This approach was then used to demonstrate trapping of magnetically labeled MDA-MB-231 cells.

ACKNOWLEDGEMENTS

All the experiments presented were performed on NanoLyon facilities. More precisely, Jérôme Degoutte and Nicolas Terrier are thanked for their technical help. This work was supported by CNRS, ANR Oncoscreen, LabEx IMUST and Région Rhône-Alpes. FST (Facultée des Sciences et des Technologies) and Collegium C2I@Lyon are also acknowledged for their contribution to build bio/nano experimental facilities. The authors thanks Institut Néel for i-PDMS magnetic characterization and fruitful discussions. They also thank C. Ménager (Laboratoire PESCA, UMR7195, Université Paris 6, France) for providing the maghemite nanoparticles. R.G. is thankful to DGA and CNRS for a PhD fellowship.

REFERENCES AND CITATIONS

[1]Hyun K.-A. & Jung H.-I. (2014). Advances and critical concerns with the microfluidic enrichments of circulating tumor cells. *Lab Chip*, **14**, 45-56.
[2]Plouffe B. D., Kniazeva T., Mayer J. E., Murthy S. K. & Sales V. L. (2009). Xx. *FASEB J.*, **23**, 3309-3314.
[3]Kang J. H., Krause S., Tobin H., Mammoto A., Kanapathipillai M. & Ingber D. E. (2012). Xx. *Lab Chip*, **12**, 2175-2181.
[4]Lin M. X., Hyun K. A., Moon H. S., Sim T. S., Lee J. G., Park J. C., Lee S. S. & Jung H. I. (2013). Xx. *Biosens. Bioelectron.*, **40**, 63-67.
[5]Alazzam A., Stiharu I., Bhat R. & Meguerditchian A. N. (2011). Xx. *Electrophoresis*, **32**, 1327-1336.
[6]An J., Lee J., Lee S. H., Park J. & Kim B. (2009). Xx. *Anal. Bioanal. Chem.*, **394**, 801-809.
[7]Jung J., Seo S. K., Joo Y. D. & han K. H. (2011). Xx. *Sens. Actuators B*, **157**, 314-320.
[8]Hyun K.-A. & Jung H.-I. (2013). Microfluidic devices for the isolation of circulating rare cells: a focus on affinity-based, dielectrophoresis and hydrophoresis. *Electrophoresis*, **34**, 1028-1041.
[9]Martinez-Duarte R. (2012), Microfabrication technologies in dielectrophoresis applications-A review. *Electrophoresis*, **33**, 3110-3132.
[10]Park B. Y. & Madou M. J. (2005). 3-D electrode designs for flow-through dielectrophoretic systems . *Electrophoresis*, **26**, 3745-3757.
[11] Jung Y., Choi Y., Han K.-H. & Frazier A. B. (2010). Six-stage cascade paramagnetic mode magnetophoretic separation system for human blood samples . *Biomed Microdev*. **12**, 637-645.
[12]Deman A.-L., Brun M., Quatresous M., Chateaux J.-F., Frenea-Robin M., Haddour N., Semet V. & Ferrigno R. (2011). Characterization of C-PDMS electrodes for electrokinetic applications in microfluidic systems. *J. Micromech. Microeng*, **21**, 095013
[13] Faivre M.,Gelszinnis R., Degouttes J., Terrier N., Rivière C., Ferrigno R. & Deman A.-L. (2014). Magnetophoretic manipulation in microsystem using i-PDMS microstructures. *Biomicrofluidics*, accepted.
[14] Niu X, Peng S, Liu L, Wen W, Sheng P. (2007). Characterizing and patterning of PDMS-based conducting composites, *Adv. Mater***. 19**, 2682-2686.

[15] Abonnenc M., Gassner A.-L., Morandini J., Josserand J., & H. H. Girault. (2009). Magnetic track array for efficient bead capture in microchannels. *Anal. Bioanal. Chem.* **395**, 747-757.
[16] Brun M., Frenea-Robin M., Chateaux J.-F., Haddour N., Deman A.-L. & Ferrigno R. (2012). A New Microfluidic Device for Electric Lysis and Separation of Cells. 34th Annual International Conference of the IEEE Engineering-in-Medicine-and-Biology-Society (EMBS), San Diego.
[17] Jin C., McFaul S. M., Duffy S. P., Deng X., Tavassoli P., Black P. C. & Ma H. (2014). Technologies for label-free separation of circulating tumor cells: from historical foundations to recent developments. *Lab. Chip.*, **14**, 32-44.